Am J Cancer Res 2025;15(11):4982-4998
www.ajcr.us /ISSN:2156-6976/ajcr0166423

Original Article

MARVELD1 as a tumor stem cell marker and therapeutic target in visceral obesity-associated ovarian cancer

Xianping Zhou[1*], Fei Wu[2*], Jiaqi Xu[2*], Longwei Qiao[3*], Yayun Zhang[2], Meng Liu[2], Guannan Feng[2], Shunyu Hou[2], Cong Shen[3], Yuting Liang[4,5]

[1]Department of Blood Transfusion, The Affiliated Bozhou Hospital of Anhui Medical University, Bozhou 236800, Anhui, China; [2]Department of Obstetrics and Gynecology, The Affiliated Suzhou Hospital of Nanjing Medical University, Gusu School, Nanjing Medical University, Suzhou Municipal Hospital, Suzhou 215002, Jiangsu, China; [3]Center for Reproduction and Genetics, School of Gusu, The Affiliated Suzhou Hospital of Nanjing Medical University, Suzhou Municipal Hospital, Nanjing Medical University, Suzhou 215000, Jiangsu, China; [4]Center for Clinical Laboratory, The First Affiliated Hospital of Soochow University, Suzhou 215000, Jiangsu, China; [5]Molecular Oncology Laboratory, Department of Orthopedic Surgery and Rehabilitation Medicine, The University of Chicago Medical Center, Chicago, IL 60637, USA. [*]Equal contributors.

Received May 28, 2025; Accepted November 25, 2025; Epub November 25, 2025; Published November 30, 2025

Abstract: Background: Visceral obesity-related genes (VORGs) have been implicated in cancer progression, but their biological and clinical relevance in ovarian cancer (OC) remains uncertain. Methods: Prognostic modeling of VORGs was carried out using the The Cancer Genome Atlas (TCGA) and GSE53963 datasets. This model was further investigated in its association with tumor immunity, immune checkpoint inhibitor (ICI) response, and chemotherapy outcomes. Additionally, single-cell data were analyzed to explore gene expression within the tumor microenvironment of this model, specifically identifying high expression of the key gene MARVELD1 in tumor stem cells. The functionality of MARVELD1 was validated experimentally through Cell Counting Kit-8 (CCK-8), transwell, and colony formation assays. Results: OC patients were stratified into four molecular subtypes based on overall survival (OS)-associated VORG expression profiles. Differentially expressed genes (DEGs) between subtypes with prognostic relevance were identified and subsequently analyzed using least absolute shrinkage and selection operator (LASSO) regression and stepwise Cox modeling, resulting in a robust four-gene prognostic model comprising CXCL9, IGF2, FCGBP, and MARVELD1. This model effectively classified patients into high- and low-risk groups, with the high-risk group demonstrating significantly poorer outcomes ($P < 0.001$). In addition, risk scores showed strong correlations with immune checkpoint gene expression and predicted chemotherapy sensitivity, underscoring their utility in forecasting therapeutic responses. Single-cell transcriptomic analysis revealed heterogeneous expression of model genes across subpopulations, with MARVELD1 prominently enriched in tumor stem cells. MARVELD1 was found to modulate early cellular processes through pathways such as reactive oxygen species. Finally, in vitro experiments confirmed that MARVELD1 knockdown significantly inhibited OC cell proliferation, invasion, and colony formation, further validating its oncogenic role. Conclusion: A VORG-based prognostic model was established that correlates with OC prognosis, tumor immune microenvironment, and treatment sensitivity. These findings suggest that MARVELD1 and related pathways may serve as potential targets to improve prognostic stratification and guide therapy in OC.

Keywords: Visceral obesity, prediction model, ovarian cancer, molecular subtypes, tumor microenvironment

Introduction

Ovarian cancer (OC) has been recognized as one of the most prevalent gynecologic malignancies, frequently associated with a poor prognosis. The primary approaches to treating OC encompass surgical intervention, chemotherapy, and targeted therapy, among others [1-3]. As mechanistic insights into OC pathogenesis have advanced, increasing emphasis has been placed on targeted therapeutic approaches. Among the most widely implemented agents are PARP inhibitors, such as olaparib, and anti-angiogenic therapies, including bevacizumab [4, 5]. Nevertheless, the clinical utility of these targeted treatments has remained limited, as

they are designed to act selectively on tumor-specific pathways and may not be universally applicable across all patient subgroups [6-8]. This limitation has underscored the urgent need for the identification of novel biomarkers that could serve as actionable targets for broader therapeutic applicability in OC.

Visceral adiposity, which serves physiological roles such as organ protection and structural support, has been shown to increase the risk of cardiovascular and metabolic disorders. In parallel, elevated levels of visceral fat have been correlated with heightened susceptibility and worse outcomes in several malignancies, including colorectal, pancreatic, and small-cell lung cancers [9-12]. These associations are thought to arise from the complex interplay between metabolic dysregulation and alterations in the tissue microenvironment, which collectively facilitate cancer initiation and progression. Previous studies have demonstrated that stromal cells derived from visceral or obesity-associated adipose tissues can promote ovarian tumor growth. Moreover, obesity has been associated with increased tumorigenesis in murine models of OC and has been linked to heightened postoperative complication rates among OC patients [13, 14]. Despite these findings, the molecular underpinnings that connect visceral obesity and the pathobiology of OC have remained poorly elucidated.

In the present study, a systematic characterization of visceral obesity-related genes (VORGs) in OC was conducted through the integration of single-cell RNA sequencing (scRNA-seq) and bulk RNA sequencing datasets. A prognostic model was developed based on the expression of key VORGs, enabling the assessment of their relevance to OC prognosis, tumor microenvironment (TME) characteristics, and therapeutic response. To further explore the functional implications of these genes, single-cell analyses were performed to examine gene expression heterogeneity within distinct cellular subpopulations. Particular attention was directed toward the role of MARVELD1 in tumor stem-like cells, and its oncogenic potential was investigated using in vitro experimental validation. Collectively, the findings presented herein have provided mechanistic insight into the contribution of visceral obesity to OC progression and have highlighted potential molecular targets for the development of precision therapies in this high-risk patient population.

Materials and methods

Acquisition of OC data

RNA-seq data and clinical information for OC patients were derived from GSE53963 and The Cancer Genome Atlas (TCGA) database. The microarray dataset GSE24883, containing mRNA expression profiles, was acquired for analysis. Differential gene expression between 8 subjects with visceral obesity and 8 lean subjects was assessed using criteria of $|\log_2$ fold change (FC)$| > 1$ and $P < 0.05$. This analysis identified differential genes, classified as VORGs. Cox regression analysis screened out 8 VORGs that were significantly correlated with OC. Kaplan-Meier (KM) method was used to evaluate the prognostic value of VORGs.

Consensus unsupervised clustering of obesity related genes

Firstly, a univariate Cox regression analysis was used to determine the differentially expressed genes (DEGs) in relation to prognosis of OC patients. Based on the expression level of VORGs, we used the R software package "ConsensusClusterPlus" to perform consensus unsupervised cluster analysis, and divided patients into different Obesity-related clusters (ORG clusters) [15]. In addition, comparison of survival probabilities of different subgroups of patients using the R software packages "Survival" and "Survival Miner" was analyzed by KM curves and log-rank tests.

Tumor immune infiltration

Single sample gene set enrichment analysis (ssGSEA) was used to detect the degree of immune infiltration of different subtypes. The ESTIMATE package serves as a tool for predicting tumor purity by estimating stromal and immune cells in malignant tissue through the utilization of expression data. It generates three scores: i) StromalScore, which documents the presence of stroma in the tumor tissue; ii) ImmunityScore, representing the infiltration of immune cells in the tumor tissue; and iii) EstimatedScore, inferring the purity of the

tumor [16, 17]. CIBERSORT algorithm was used to quantify the immune infiltration of different groups [18].

Construction of the obesity related prognostic model

Then, to improve the accuracy of prediction, we performed least absolute shrinkage and selection operator (LASSO) regression shipping and stepwise Cox regression analysis to construct a 4-gene signature. Patients in the TCGA and GSE53963 databases were randomized into a training group (n = 297) and a test group (n = 297). We calculated the risk score (risk score = expression * coefficient for each gene). Based on the median value derived from the risk score, patients were categorized into high-risk and low-risk groups. To assess the prognostic predictive reliability of the risk scoring system, overall survival (OS) was explored using KM analysis and time-dependent receiver operating characteristic curves (ROCs) were plotted using "survivalROC" from the R software package.

Comprehensive analysis of pathways, TME, immune checkpoints, TIDE and chemotherapy effects

We used the Kyoto Encyclopedia of Genes and Genomes (KEGG) pathway enrichment analysis to explore the biological function of VORGs [19, 20]. Wilcoxon test was used to compare the immune checkpoint gene expression between two groups. Using the pRRophetic R package in R (version 4.1.0), the IC50 of molecular therapy and chemotherapy was calculated, and then the difference between two groups was compared [21, 22].

Single-cell RNA sequencing data analysis

Download the RNA-seq dataset GSE184880 from the GEO database for analysis. We analyzed the RNA-seq dataset using the RSeurat software package, retaining cells containing ≤ 10% mitochondrial genes [23]. At the same time, we filtered out cells with a gene number (nFeature RNA) ≤ 300 or ≥ 5000. After scaling gene expression levels, we normalized the data using the LogNormalize function, performed principal component analysis (PCA), and completed cell cluster labeling using the SingleR software package.

Cell culture and short interfering RNA (siRNA) cell transfection

OC cell lines OVCAR3 and A2780 were purchased from the Meisen CTCC (Hangzhou, Zhejiang, China). OVCAR3 were cultured in RPMI-1640 medium (Gibco, USA) supplemented with 20% fetal bovine serum (Excell Bio, New Zealand) and 1% penicillin-streptomycin (NCM, China) at 37°C in an incubator with 5% CO_2. Unlike OVCAR3, A2780 was cultured in RPMI-1640 medium containing 10% fetal bovine serum. All siRNAs were obtained from GenePharma (Suzhou, Jiangsu, China) and transfected into cells using Lipofectamine 2000 (Invitrogen, Carlsbad, CA, USA) following the manufacturer's instructions. The siRNAs used were as follows: MARVELD1 siRNA 1# 5'-CCGGCAUCAUGAGCGACCA-3'; MARVELD1 siRNA 2# 5'-GCUGCCUUCUGGAUCACUA-3'; NC siRNA 5'-UUCUCCGAACGUGUCACGU-3'.

RNA extraction and reverse-transcription quantitative PCR (RT-qPCR)

Total RNA was extracted with TRIzol (Vazyme) according to the manufacturer's instructions. Total RNA was reverse-transcribed into cDNA using HiScript III RT Super Mix with a qPCR kit (R323-01, Vazyme). Real-time PCR was performed on a 7500 system (Applied Biosystems, Foster City, CA, USA) with SYBR Green Master Mix (Novoprotein Scientific Inc., Shanghai, China). We normalized the relative level of gene expression to that of 18s rRNA by the $2^{-\Delta\Delta Ct}$ method. The primers used were as follows: MARVELD1 5'-TTGTGCTCACTCTGTCTGCC-3' and 5'-GACCTATGCAACTGCCTCCA-3'; 18s rRNA 5'-AAACGGCTACCACATCCAAG-3' and 5'-CCTCCAATGGATCCTCGTTA-3'. All primers were synthesized by Beijing Tsingke Biotech Co., Ltd.

Cell proliferation and migration assays

Cells were plated at a density of 2500 cells per well in 96-well plates. At different points in time, we added 20 μl Cell Counting Kit-8 (CCK-8) solution (Beyotime Institute of Biotechnology, Nantong, Jiangsu, China) to each well and incubate for 4 h, as previously described [24]. Then we use a microplate reader (Bio-Rad Model 680, Richmond, CA, USA) to evaluate Cells at 450 nm. For the colony formation tests, 1000 cells were seeded into six-well plates and cultured for 2 weeks. The colonies were fixed with

methanol for 15 min, stained with 0.1% crystal violet (Beyotime) for 30 min, and counted under a bright-field microscope (Carl Zeiss, Oberkochen, Germany). To detect cell migration ability, we used a transwell assay. Transfected cells were seeded into the upper chamber at a density of 50000 cells per well (Corning, NY 14831, USA). After 48 h the cells on the lower membrane were immobilized and stained as previously described.

Statistical analysis

The analysis and manipulation of data were executed utilizing R 4.1.0, in conjunction with RStudio version 4.1.0 as the integrated development environment. To determine related genes and their prognostic value, univariate Cox regression analysis was performed. The survival analysis was conducted via the KM method, and log-rank tests were employed to identify the significance of differences. Correlation coefficients were evaluated by Spearman analysis. Wilcoxon test was used for comparisons between two groups. One-way ANOVA and Kruskal-Wallis tests were used for comparisons across multiple groups. For datasets involving continuous time points (such as cell proliferation assays), Repeated Measures ANOVA was performed to account for the correlation between repeated measurements within the same sample. Data were expressed as mean ± standard deviation (SD). $P < 0.05$ was considered significant.

Results

Gene alterations and transcriptional expression of VORGs in OC

A total of 42 differentially expressed VORGs were initially identified from the GSE24883 dataset by applying a significance threshold of $P < 0.05$ and $|\log_2 FC| > 1$. Subsequently, univariate Cox regression analysis was conducted, and eight VORGs were found to be significantly associated with OS in patients with OC (**Figure 1A**). These genes included TRIM13, BAG3, HOXC9, ZBP1, MED13L, MAPT, PYHIN1, and ZNF146, with several functioning as either risk or protective factors. Furthermore, somatic mutations analysis in these eight VORGs revealed a mutation frequency of 5.41% in 462 OC patients from the TCGA cohort (Figure S1A). Copy number variation (CNV) analysis of eight VORGs, showing ZNF146 with the most frequent amplifications, while BAG3 and MED13L exhibited the highest deletion rates (Figure S1C). Using the expression profiles of these eight prognostic VORGs, consensus clustering was performed on samples from the TCGA and GSE53963 cohorts. As a result, four distinct molecular subtypes (Clusters A-D) were delineated (**Figure 1B**). The heatmap visualization illustrated clear subtype-specific expression patterns and their relationships with clinicopathological features. Of note, Cluster D was characterized by elevated expression of TRIM13, BAG3, MED13L, and ZNF146, which was associated with high-grade tumors and increased mortality.

To assess the clinical significance of these subtypes, KM survival analysis was carried out. Significant differences in OS were observed among the four clusters ($P < 0.001$ by log-rank test), with Cluster A exhibiting the most favorable prognosis and Cluster D the least favorable (**Figure 1C**). Accordingly, Clusters A and D were selected for further comparative analysis. Differential gene expression analysis between Clusters A and D identified 970 DEGs. KEGG pathway enrichment analysis revealed that Cluster A was primarily enriched for oxidative phosphorylation and xenobiotic/drug metabolism pathways, particularly those mediated by cytochrome P450 enzymes. In contrast, Cluster D showed significant enrichment in the neurotrophin signaling pathway and ERBB signaling pathway, both of which are associated with tumor progression and resistance to therapy (**Figure 1D**).

Lastly, the immune landscape across the molecular subtypes was evaluated using ssGSEA. Cluster D was found to have significantly higher levels of immune infiltration across multiple immune cell types - including activated dendritic cells, eosinophils, immature B cells, mast cells, regulatory T cells, and type 1 T helper cells - compared to Cluster A (**Figure 1E**). These results indicate that the VORGs-defined subtypes are associated with distinct tumor immune microenvironments.

Construction and evaluation of VORGs prognostic model

To investigate the prognostic relevance of DEGs between molecular subtypes A and D, univari-

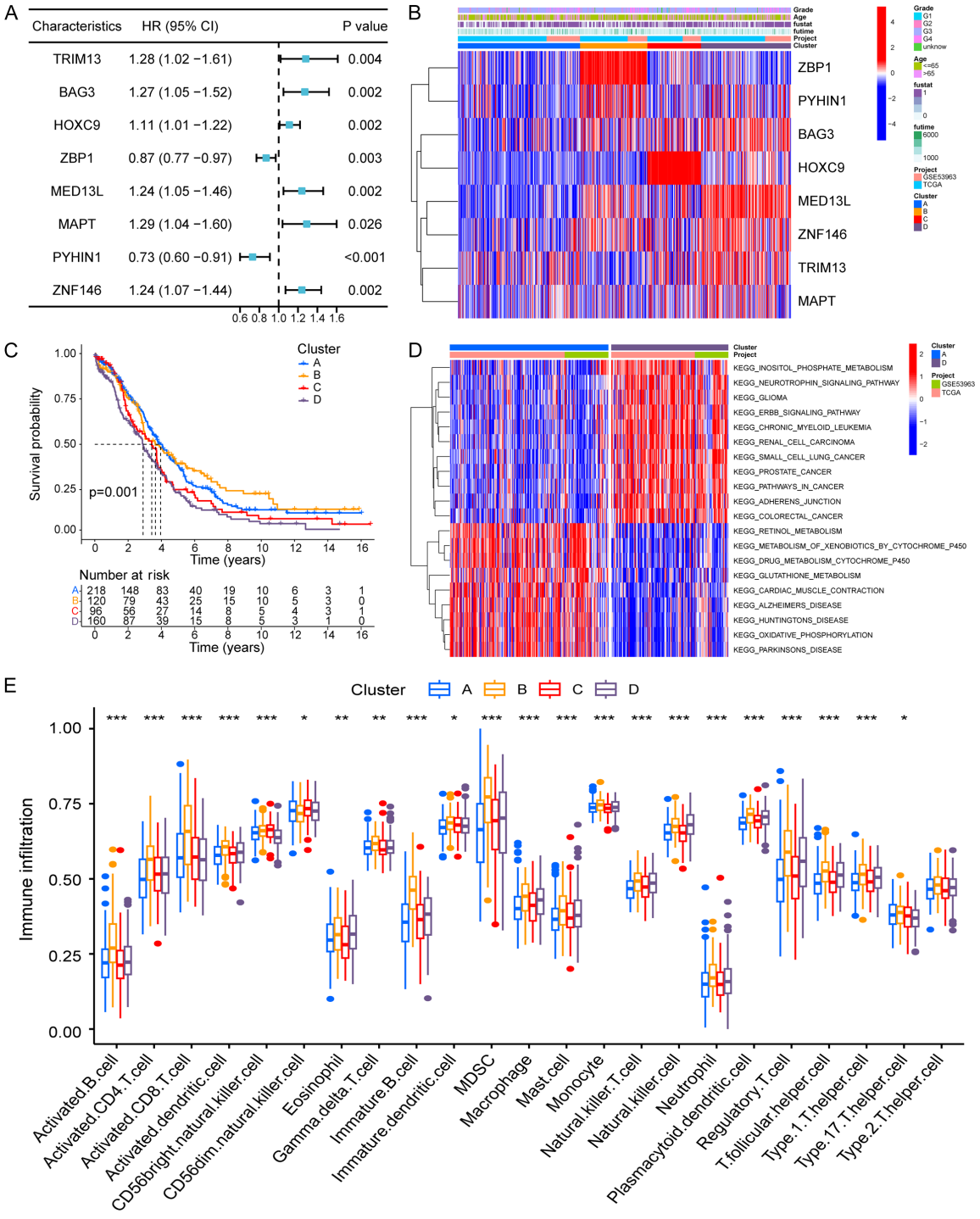

Figure 1. Gene alterations and transcriptional expression of visceral obesity-related genes (VORGs) in ovarian cancer (OC). A. Cox regression analysis of obesity-related genes and OC. B. The heat map presented the expression patterns of VORGs in conjunction with clinicopathological factors. C. Kaplan-Meier (KM) survival analysis of different subtypes. D. Kyoto Encyclopedia of Genes and Genomes (KEGG) enrichment analysis of different subtypes. E. The immune infiltration score of VORG subtypes was analyzed by single sample gene set enrichment analysis (ssGSEA). *P < 0.05, **P < 0.01, ***P < 0.001.

ate Cox regression analysis was performed on 970 DEGs. This analysis identified 336 genes significantly associated with OS (OS-related DEGs; P < 0.05). Based on the expression pro-

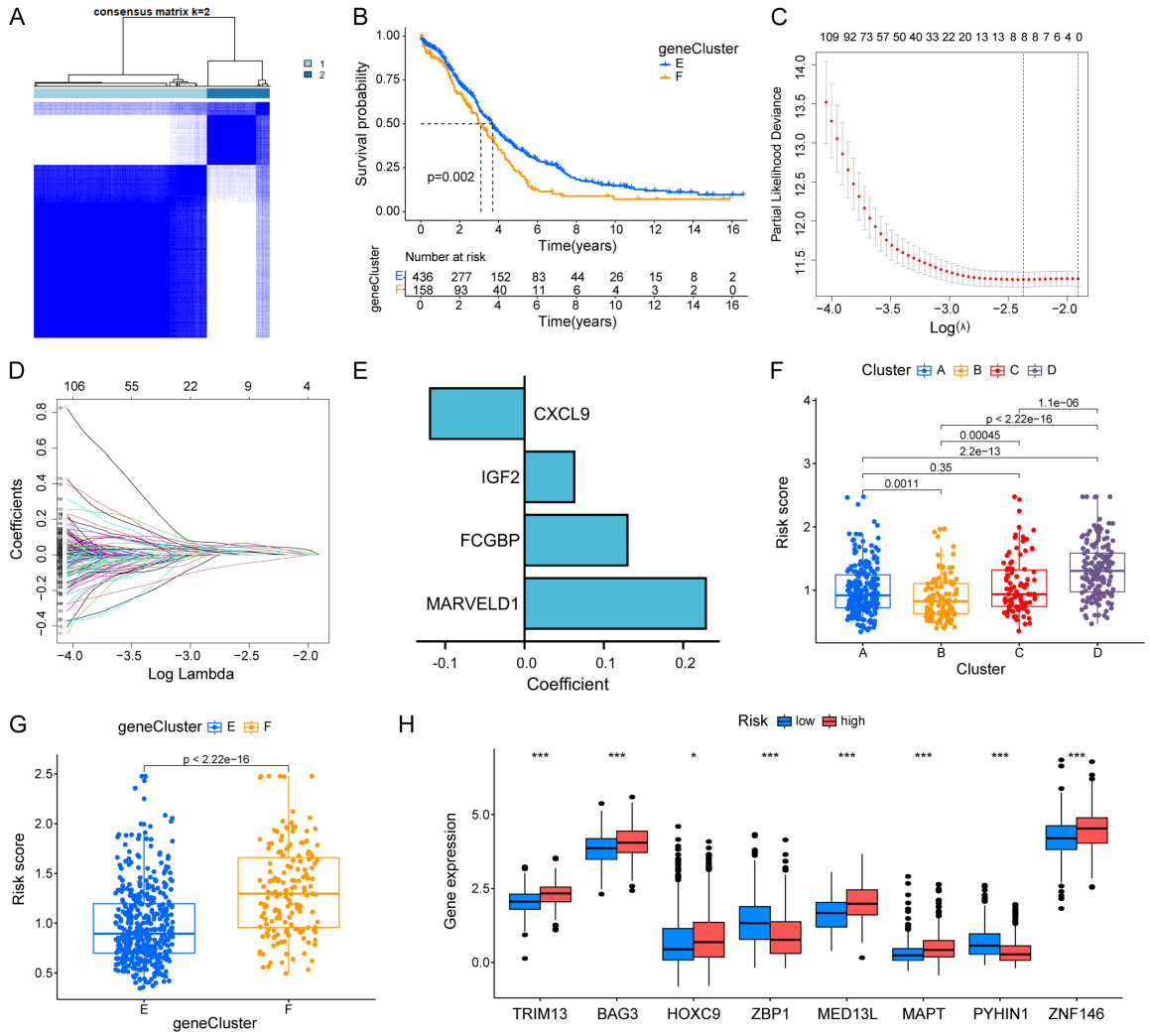

Figure 2. Identification of gene clusters in OC. A. Two gene clusters were identified using consensus cluster analysis based on the expression profiles of 336 overall survival (OS)-related DEGs. B. KM survival analysis of two gene clusters. C-E. Four differential genes were screened by least absolute shrinkage and selection operator (LASSO) regression analysis (CXCL9, IGF2, FCGBP and MARVELD1). F, G. The relationship between VORGs clusters, gene clusters, and prognostic model scores. H. The expression of VORGs were predominantly up-regulated in OC high-risk group. *P < 0.05, ***P < 0.001.

files of these genes, unsupervised clustering was applied to categorize OC patients into two transcriptional subgroups, designated as gene Cluster E and gene Cluster F (**Figure 2A**). Notably, KM survival analysis demonstrated that gene Cluster E had significantly better survival outcomes than gene Cluster F (**Figure 2B**).

To further refine the prognostic signature, the 336 OS-related DEGs were subjected to LASSO regression followed by stepwise multivariate Cox modeling. Through this iterative process, four core prognostic genes- CXCL9, IGF2, FCGBP, and MARVELD1 - were identified (**Figure 2C-E**). These genes were subsequently used to construct a multigene prognostic model. Analysis of somatic mutations in these model genes revealed a mutation frequency of 4.76% (Figure S1B). CNV profiling demonstrated prominent CNV alterations involving all four genes, with FCGBP displaying the most frequent amplifications, while IGF2 showed the highest deletion rates, further underscoring their genomic instability (Figure S1D).

The relationships among VORG-defined molecular subtypes, gene clusters, and the prognostic model were next explored. Risk scores

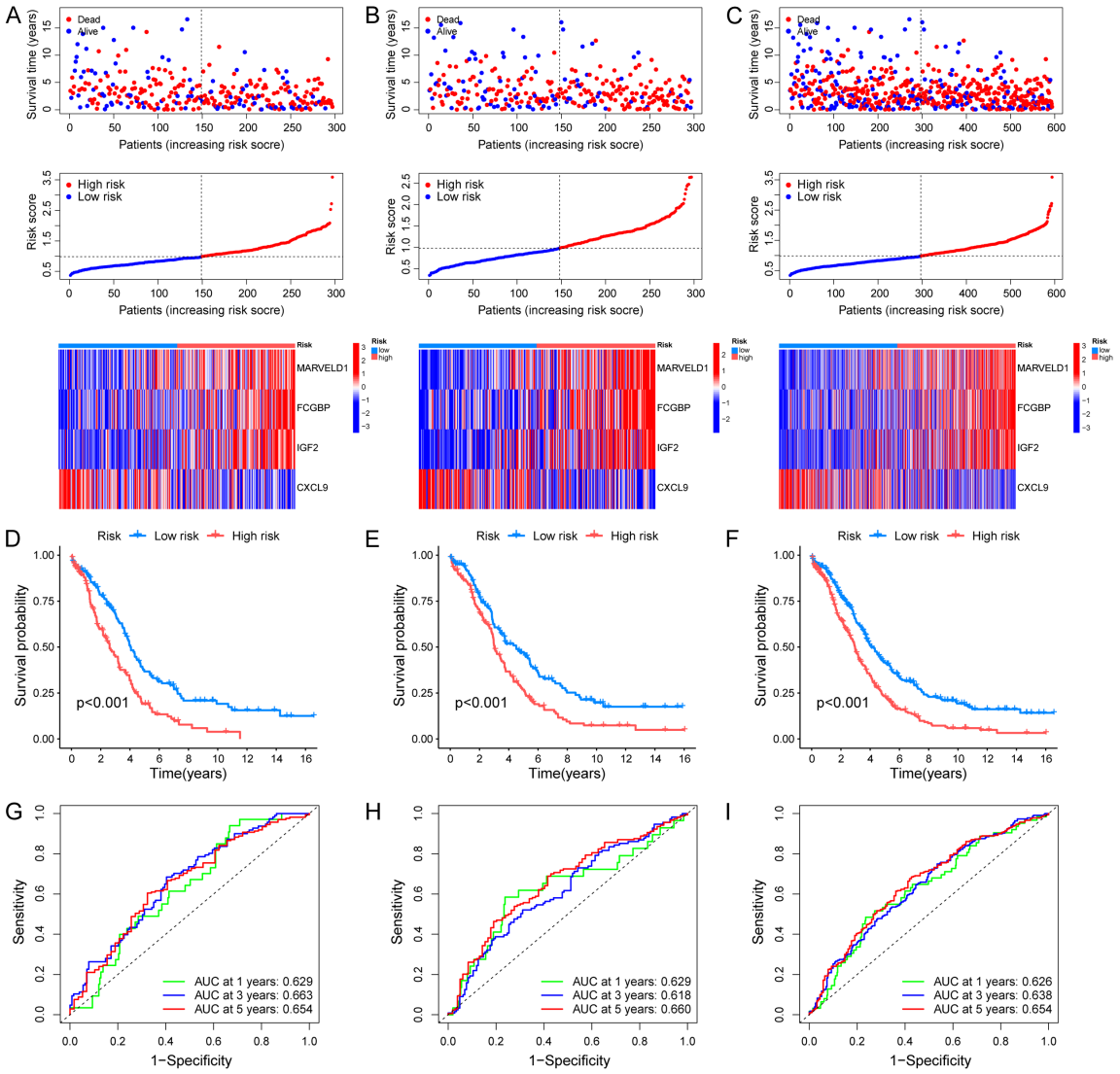

Figure 3. Evaluation of the VORG prognostic model. A-F. Patients in the high-risk group had significantly worse OS compared to those in the low-risk group. G-I. Receiver operating characteristic curves (ROCs) curves showcased 1-, 3-, and 5-year AUC values within the ranges of 0.629-0.663, 0.618-0.660, and 0.626-0.654 for the training, testing, and all groups respectively.

derived from the four-gene model were found to be significantly elevated in VORGs Cluster D compared to Cluster A (**Figure 2F**). Similarly, risk scores in gene Cluster F were markedly higher than those in Cluster E (**Figure 2G**), indicating a consistent pattern across transcriptomic and genomic layers. Patients were then stratified into high-risk and low-risk groups using the median risk score as the cutoff. Expression analysis revealed that VORGs were predominantly and markedly upregulated in the high-risk group, suggesting a tight association between elevated VORGs expression, higher risk scores, and more aggressive tumor phenotypes (**Figure 2H**). These findings indicate that the integrative prognostic model not only reflects transcriptomic alterations but also captures biologically and clinically meaningful heterogeneity in OC.

To assess the predictive performance of the four-gene prognostic signature, survival risk stratification was evaluated across the training cohort, internal testing cohort, and the entire cohort. In all three groups, patients classified into the high-risk category exhibited significantly reduced OS compared to those in the low-risk group, as demonstrated by KM analysis (**Figure**

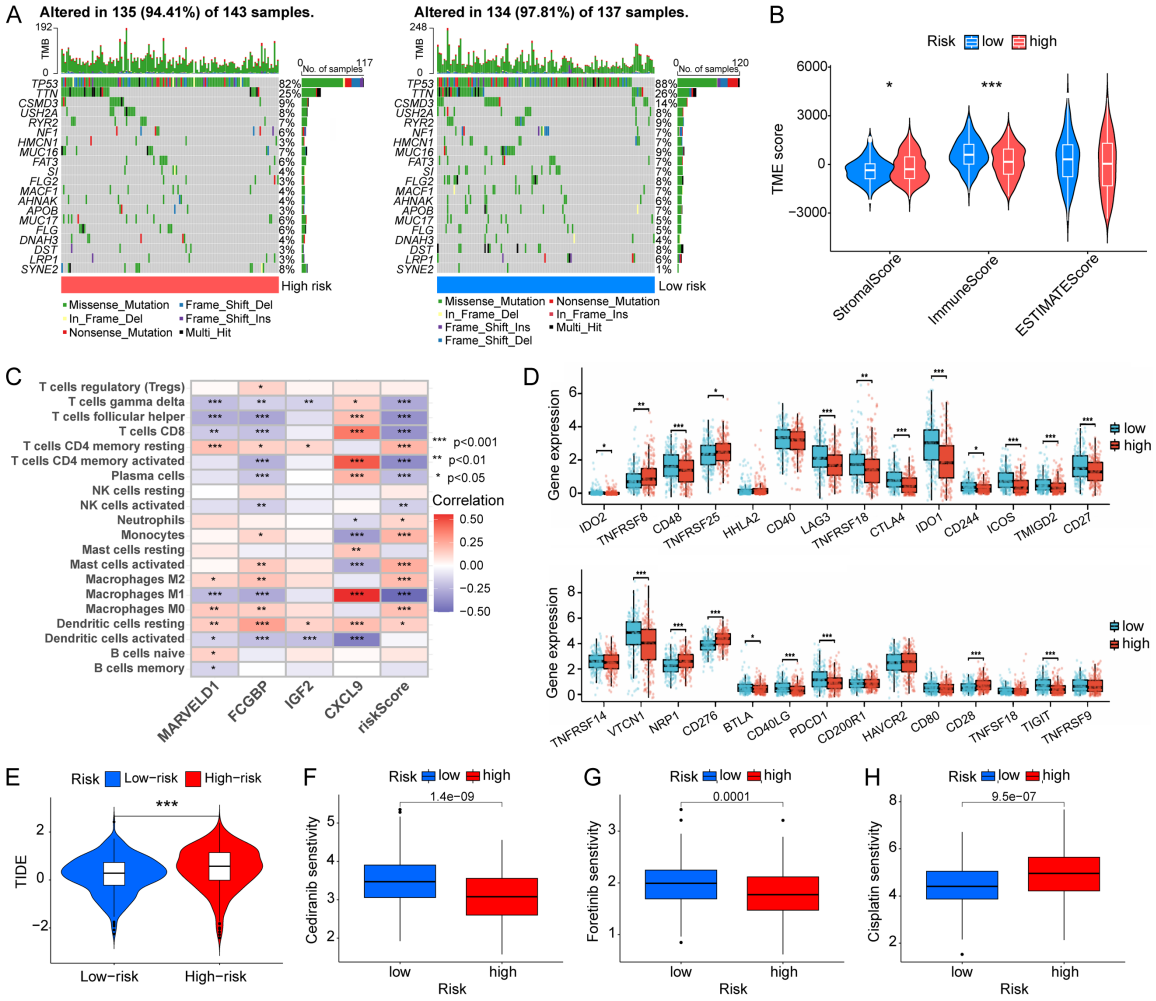

Figure 4. Analysis of immune checkpoint expression, stromal scores and immunotherapy and chemotherapy predictions. A. Assessment of gene mutation levels between high and low risk groups. B. Comparison of tumor microenvironment (TME) scores between the two groups. C. Degree of immune infiltration of risk genes. D. The expression of immune checkpoint genes was different in high-risk group and low-risk group. E. Comparison of TIDE scores between different groups. F-H. Comparison of drug treatment effect between high-risk group and low-risk group. *P < 0.05, **P < 0.01, ***P < 0.001.

3A-F). This consistent pattern underscores the model's prognostic robustness across different datasets. Time-dependent ROC curves were generated to further evaluate the model's discriminatory capacity. The AUC values for predicting 1-, 3-, and 5-year OS were 0.629, 0.663, and 0.654 in the training set; 0.629, 0.618, and 0.660 in the testing set; and 0.626, 0.638, and 0.654 in the full cohort, respectively (**Figure 3G-I**). These moderate but consistent AUCs confirmed the model's stability and predictive applicability across multiple temporal endpoints.

In culmination, an inter-VORGs network was constructed to unveil the association between VORGs and the prognostic model's significance in OC, with MARVELD1 occupying a central position within this network (Figure S1E).

Integrative analysis of the prognostic model with genomic alterations, immune landscape, and therapeutic response

To elucidate the genomic characteristics associated with different risk groups, the mutational landscape of OC patients was profiled across high- and low-risk subgroups. As illustrated in **Figure 4A**, a notably higher mutation frequency was observed in the low-risk group, suggesting distinct genomic architectures between the two prognostic strata.

To further explore the relationship between the prognostic signature and the tumor immune microenvironment, TME scores were compared. The high-risk group exhibited a significantly elevated StromalScore, indicating a more stroma-rich tumor microenvironment, while the ImmuneScore was slightly lower and the EstimateScore showed no significant difference (**Figure 4B**). Immune cell infiltration was then analyzed using correlation analyses between immune cell types, risk scores, and the expression of the four model genes. The risk score was positively correlated with resting CD4 memory T cells, monocytes, and activated mast cells infiltration, and negatively correlated with CD8 T cells, activated CD4 memory T cells, and plasma cells infiltration (Figure S2). Among the four genes, MARVELD1 displayed the strongest concordance with overall immune infiltration patterns (**Figure 4C**).

To assess the implications of risk stratification on immunotherapy responsiveness, we examined the expression profiles of key immune checkpoint molecules. A substantial upregulation of checkpoint-related genes - such as CD48, LAG3, TNFRSF18, CTLA4, IDO1, ICOS, TMIGD2, CD27, VTCN1, PDCD1, and TIGIT - was detected in the low-risk group (**Figure 4D**). This elevated checkpoint expression reflects the "immune-hot" nature of the TME, typically indicative of significant T-cell activation and infiltration. In addition, the Tumor Immune Dysfunction and Exclusion (TIDE) algorithm was employed to evaluate immune evasion potential. Despite high checkpoint expression, TIDE scores were significantly lower in the low-risk group, suggesting that immune escape mechanisms are less pronounced and that T-cells retain functionality. This finding suggests a more permissive TME, which may be more responsive to immune checkpoint blockade therapy. In contrast, the high-risk group exhibited significantly higher TIDE scores, reflecting more pronounced immune escape mechanisms, such as T-cell exhaustion or exclusion. These immune dysfunctions contribute to impaired immune surveillance, rendering the tumor less responsive to immune checkpoint inhibitors (**Figure 4E**).

Drug sensitivity analysis further revealed that compared to the low-risk group, the high-risk group demonstrated increased predicted sensitivity to angiogenesis inhibitors such as cediranib and foretinib, along with reduced sensitivity to cisplatin (**Figure 4F-H**). These observations highlight the potential utility of the prognostic model in guiding personalized therapeutic strategies, including the selection of targeted agents and cytotoxic chemotherapy.

Functional analysis of 4 prognostic model genes in scRNA seq data

To delineate the cellular origin and functional implications of the prognostic gene signature, we leveraged the OC scRNA-seq dataset GSE184880. Unsupervised clustering and Uniform Manifold Approximation and Projection (UMAP) dimensionality reduction identified a heterogeneous tumor ecosystem composed of mesenchymal stem cells (MSCs), fibroblasts, macrophages, epithelial cells, tissue stem cells, and other cell types (**Figure 5A**). Tissue stem cells refer to a cell population characterized by high expression of stemness-related genes. In normal tissues, these cells represent normal stem cells with self-renewal and differentiation potential. In tumor tissues, we refer to them as "malignant stem-like cells" due to their enrichment in the cancer microenvironment and potential role in driving tumorigenesis. Expression mapping of the four signature genes - CXCL9, IGF2, FCGBP, and MARVELD1 - demonstrated distinct cell-type specificity, with MARVELD1 exhibiting particularly broad and high expression in MSCs, macrophages, fibroblasts, epithelial cells, and tissue stem cells (**Figure 5B**, **5C**).

Comparative analyses between normal and cancer samples revealed a significant elevation of MARVELD1 in malignant tissue, especially within tissue stem cells (**Figure 5D-F**). This observation suggested a potential role of MARVELD1 in stem-like compartments contributing to tumorigenesis.

To further dissect the heterogeneity within tissue stem cells, we stratified these cells into MARVELD1-high and MARVELD1-low groups based on mean expression levels. UMAP analysis revealed distinct spatial segregation of these subpopulations (**Figure 6A**), with MARVELD1-high cells markedly enriched in cancer-derived tissues (**Figure 6B**). This enrichment implicates MARVELD1 as a potential determinant of malignant stem-like cell identity.

Gene Ontology (GO) enrichment analysis of DEGs between the two subgroups highlighted

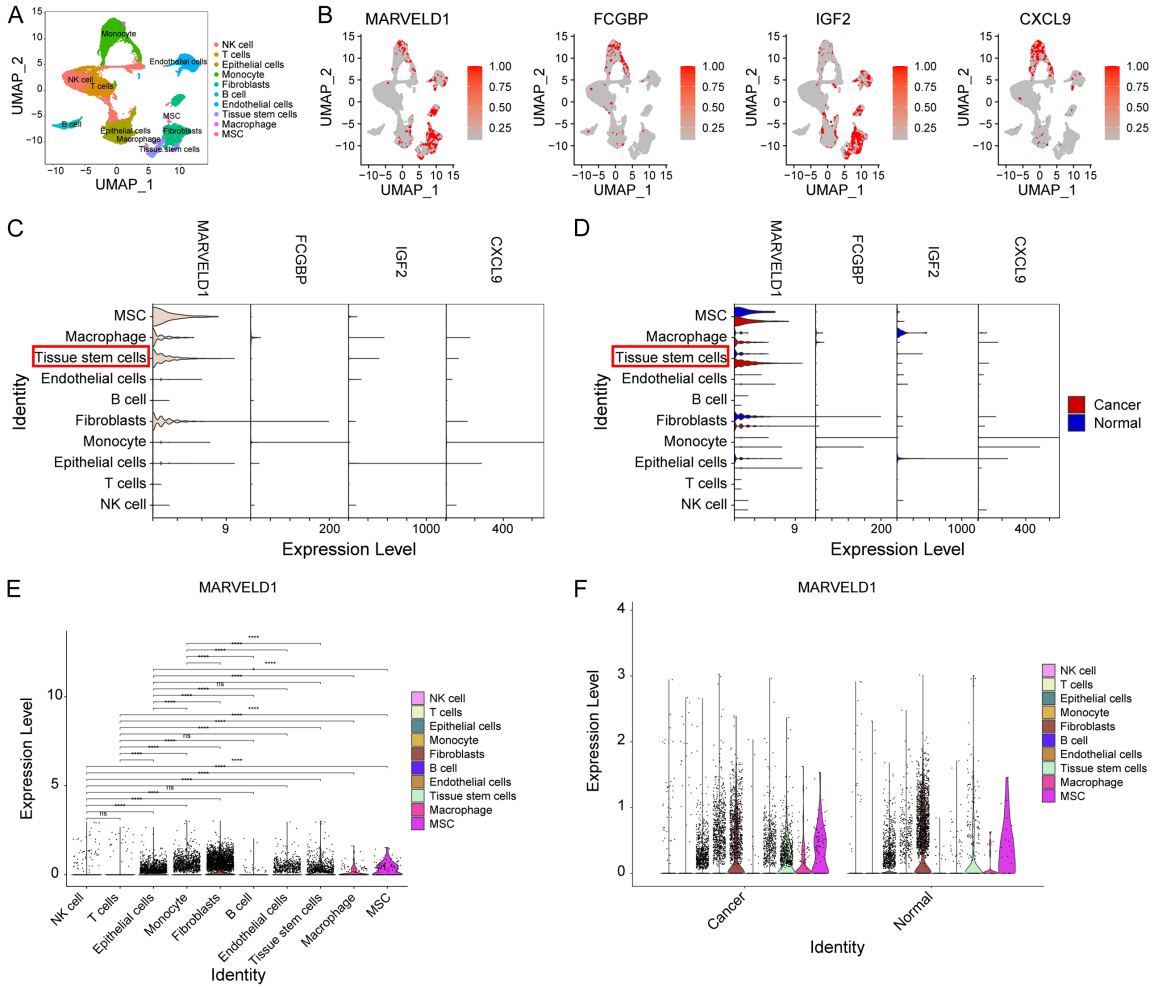

Figure 5. Analysis of single-cell subsets of OC. A. Annotation of all cell types in GSE184880. B. Expression of CXCL9, IGF2, FCGBP and MARVELD1 in each cell type. C-F. Cell localization of differential genes in OC tissue species. ns, P > 0.05; *P < 0.05, ****P < 0.0001.

pathways associated with ribosomal structure, electron transport activity, and oxidoreduction-driven transmembrane transporter functions (**Figure 6C**). KEGG pathway analysis revealed prominent associations of MARVELD1 with oxidative phosphorylation, Parkinson's disease, and prion disease, underscoring its mitochondrial and metabolic regulatory roles (**Figure 6D**). Furthermore, immune-related gene set enrichment analysis (irGSEA) indicated that MARVELD1-high tissue stem cells displayed inhibition of angiogenesis, along with activation of the unfolded protein response, reactive oxygen species (ROS) pathways, protein secretion, and PI3K-AKT-mTOR signaling (**Figure 6E**). Collectively, these findings suggest that MARVELD1 delineates a functionally distinct subpopulation of tumor-propagating stem-like cells with heightened metabolic activity and immune-modulating capacity.

MARVELD1 promotes the proliferation and migration ability of OC cells

In our analysis, MARVELD1 emerged as the factor most closely linked to OC, prompting our speculation regarding the cancer-promoting potential of the obesity-related gene MARVELD1 in OC. Subsequently, we sought to validate the cancer-promoting phenotype of MARVELD1 in two OC cell lines, namely OVCAR3 and A2780. Our approach commenced by transfecting these cells with both negative control (NC) and two distinct types of siRNA, thereby enabling us to gauge the efficiency of MARVELD1 knockdown through RT-qPCR (**Figure 7A**, **7B**).

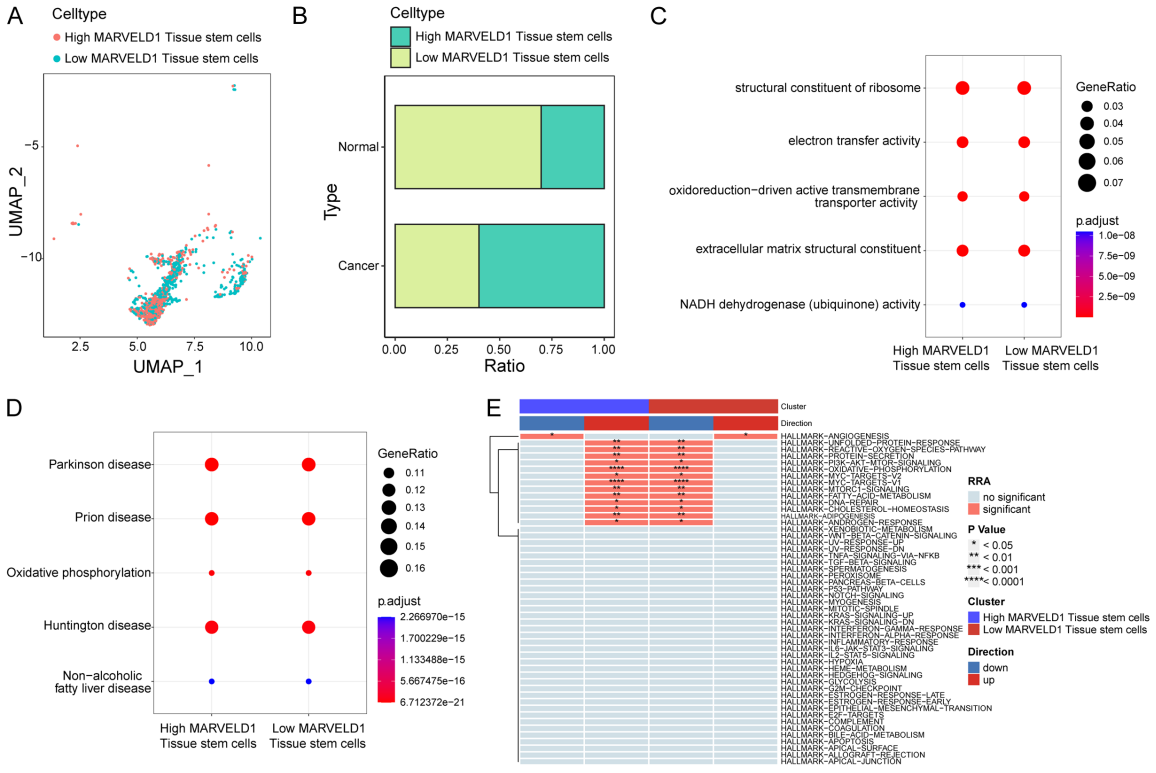

Figure 6. Validation of single-cell RNA sequencing. A. Uniform Manifold Approximation and Projection (UMAP) analysis of MARVELD1 high and low expression groups. B. Distribution of MARVELD1 high-low expression group in OC tissue and para-cancer samples. C-E. Relationship between MARVELD1 expression and cell function.

Following this, a CCK-8 experiment was undertaken, revealing a substantial attenuation in the proliferation ability of OC cells after MARVELD1 knockdown (**Figure 7C**, **7D**). Furthermore, the colony formation experiment unveiled a notable reduction in the number of colonies formed upon MARVELD1 knockdown, relative to the NC group (**Figure 7E**, **7F**). In addition, the transwell assay demonstrated a significant decrease in the migration capacity of OC cells upon MARVELD1 silencing (**Figure 7G**, **7H**). Collectively, the outcomes of these cell function experiments collectively highlight the role of MARVELD1 in promoting the progression of OC.

Discussion

Visceral obesity has been identified as a significant factor in the development of various diseases, including complex disease phenotypes such as Crohn's disease and tumor progression [25, 26]. Research has shown that visceral obesity induces an overactive state of platelets, which, in turn, influences the onset and metastasis of colon cancer by secreting growth factors and cytokines such as TGF-β and PDGF7, and through direct interaction with cancer cells and endothelium [27]. Additionally, a Mendelian randomization study has suggested that visceral fat is a potential driver for an increased risk of OC, particularly in tissue types like endometrioid and clear cell OC [28]. Nevertheless, the precise mechanisms and associations between visceral obesity and metabolic processes in OC remain inadequately elucidated [29, 30]. A systematic investigation was conducted to explore the molecular characteristics of VORG expression in OC. Two distinct VORG subtypes with significantly different prognostic outcomes were identified. Based on the selected VORGs, a four-gene prognostic model comprising CXCL9, IGF2, FCGBP, and MARVELD1 was constructed. This model enabled the reliable stratification of patients into high- and low-risk subgroups. Notably, significant differences were observed in immune infiltration profiles and immune checkpoint expression between the subgroups. The low-risk group was characterized by an "inflamed"

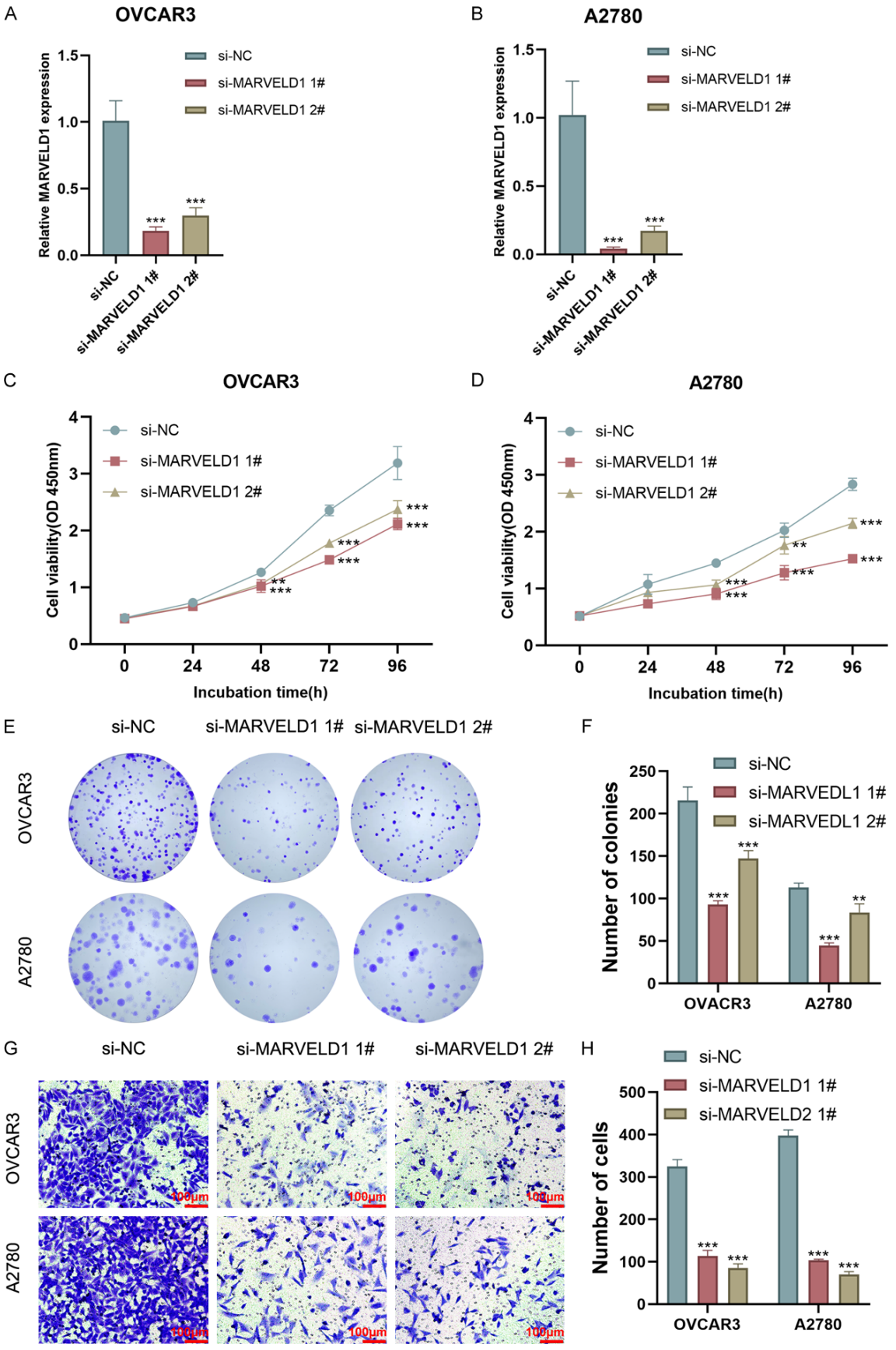
A
OVCAR3
Relative MARVELD1 expression
si-NC
si-MARVELD1 1#
si-MARVELD1 2#
B
A2780
C
OVCAR3
Cell viability(OD 450nm)
Incubation time(h)
D
A2780
E
si-NC
si-MARVELD1 1#
si-MARVELD1 2#
OVCAR3
A2780
F
Number of colonies
si-NC
si-MARVEDL1 1#
si-MARVEDL1 2#
OVACR3
A2780
G
si-NC
si-MARVELD1 1#
si-MARVELD1 2#
OVCAR3
A2780
100μm
H
Number of cells
si-NC
si-MARVELD1 1#
si-MARVELD2 1#
OVCAR3
A2780

Figure 7. MARVELD1 promotes the migration and proliferation of OC cells. A, B. Reverse transcription quantitative polymerase chain reaction (RT-qPCR) was used to verify cell knock-down efficiency. C, D. Cell Counting Kit-8 (CCK-8) suggested that the proliferation of OC cells decreased after MARVELD1 silencing. E, F. The number of clones in the si-MARVELD1 group was significantly lower than that in the NC group. G, H. Transwell assay showed that the migration ability of the si-MARVELD1 group cells was reduced (200×). Scale bar: 100 μm. **P < 0.01, ***P < 0.001.

immune microenvironment, whereas the high-risk group exhibited higher TIDE scores, indicating enhanced immune escape potential. scRNA-seq analysis revealed that MARVELD1 was specifically overexpressed in tumor stem-like cell subpopulations, with enrichment in metabolic and immune-related pathways. The pro-oncogenic role of MARVELD1 was further confirmed through functional experiments. Collectively, these findings elucidated the link between obesity-related molecular subtypes and the development of OC, providing novel insights into disease stratification and therapeutic decision-making.

Through Cox regression analysis, we identified eight VORGs that exhibited significant correlations with OC. Notably, one of these genes, BAG3, has been demonstrated to enhance platinum-resistant OC by epigenetically upregulating GALNT10 through WDR5 [31]. Additionally, another VORG, ZBP1, regulates necrotic apoptosis in OC via the RIP3/MLKL pathway [32]. Subsequently, we categorized OC patients into four distinct clusters based on the expression levels of 8 VORGs. Subsequently, KM survival analysis revealed that the prognosis of patients in group A was significantly more favorable than that of patients in group D. Further analysis using KEGG enrichment demonstrated that subtype A was primarily associated with oxidative phosphorylation and cell metabolism of drugs, suggesting that the activation of these pathways may serve as a predictive indicator for improved OC outcomes. Furthermore, our analysis using ssGSEA unveiled that subtype D exhibited elevated immune infiltration scores in activated dendritic cells, eosinophils, immature B cells, mast cells, regulatory T cells, and type 1 T helper cells. Despite this high immune cell infiltration, subtype D likely reflects an immune-suppressive or dysregulated immune state, promoting tumor immune evasion rather than effective immune surveillance.

We performed an analysis of 970 DEGs between subtypes A and D, utilizing univariate Cox regression, leading to the identification of 336 OS-related genes (P < 0.05). Subsequently, OC patients were categorized into gene Clusters E and F based on these OS-related DEGs through unsupervised cluster analysis. Notably, Cluster E displayed a more favorable prognosis (**Figure 2B**). Employing LASSO and stepwise Cox regression, we selected four pivotal genes: CXCL9, IGF2, FCGBP, and MARVELD1, for constructing prognostic models. CXCL9, a chemokine, is associated with B cell function and can modify the tumor immune microenvironment in breast cancer, with high CXCL9 levels improving outcomes in triple-negative subtypes [33]. IGF2, an insulin-like growth factor primarily secreted by the liver, is overexpressed in various cancers and linked to poor prognosis [34]. MARVELD1, a nuclear protein with MARVEL domains, plays a significant role in cancer [35, 36]. Concurrently, OC patients were stratified into high-risk and low-risk groups based on the risk score. The results indicated that VORG expression was upregulated in the high-risk group, suggesting a close association between high-risk scores and elevated VORG expression in OC.

Cancer immune surveillance refers to the process by which the immune system identifies and manages nascent tumor cells [37]. Currently, various immunotherapy approaches aim to tackle heightened immunosuppression, encompassing immune checkpoint blockade, antibody-based therapy, cancer vaccines, cytokines, adoptive cell transfer, and chimeric antigen receptor-modified T cells [38]. In this study, we assessed the expression levels of immune checkpoint genes in two patient groups, revealing elevated CD48 and LAG3 expression in the low-risk group. The low-risk group was characterized by an “inflamed” immune microenvironment with substantial infiltration of activated T cells, leading to upregulated checkpoint expression. Importantly, these T cells maintained functional capacity as evidenced by lower TIDE scores, creating an optimal environment for immunotherapy. In contrast, the high-risk group exhibited higher TIDE scores, indicating more profound immune escape mechanisms through T-cell exhaustion or exclusion, resulting in poor responsiveness to checkpoint inhibitors. These

findings expand our understanding of OC immunotherapy and the intricate interplay between visceral obesity and OC. Furthermore, the high-risk group displayed enhanced sensitivity to cediranib and foretinib but reduced sensitivity to cisplatin relative to the low-risk group, underlining the prognostic model's relevance for drug efficacy.

In this study, scRNA-seq results reveal robust MARVELD1 expression across various cell types, notably elevated in tissue stem cells within tumor samples, underscoring its close association with OC. However, a limitation of our current single-cell analysis is the lack of explicit annotation of malignant tumor cells as an independent cluster. Future research should incorporate computational methods such as inferred copy number variation (inferCNV) to clearly annotate tumor cells, enabling precise identification of malignant cells at the single-cell level. This would allow for direct validation of the expression patterns of MARVELD1 in malignant tumor versus benign epithelial cell populations. MARVELD1, a member of the MARVEL domain-containing protein family, exhibits tumor suppressor activity in breast, cervical, prostate, hepatocellular, and other cancers [39-42]. However, emerging evidence also supports a pro-cancer function of MARVELD1. For example, MARVELD1 has been shown to promote the invasiveness of pancreatic adenocarcinoma by activating epithelial-mesenchymal transition [43], and Xia et al. demonstrated that the upregulation of MARVELD1 through activation of the JAK/STAT signaling pathway contributes to the malignant phenotype of glioma cancer cells [44]. Thus, the function of MARVELD1 may be influenced by the TME, genetic background, or cell-type-specific signaling pathways, which likely accounts for its differential roles across various tumor types. Recent studies have reported an elevation in MARVELD1 expression in OC, which aligns with our findings [45]. We propose that MARVELD1 plays a pro-cancer role in OC, where its increased expression may be closely linked to tumorigenesis and the maintenance of stem cell properties. KEGG and irGSEA analyses highlight significant associations between MARVELD1 and Parkinson's disease, prion disease, oxidative phosphorylation, along with activation of unfolded protein response, ROS pathways, protein secretion, and the PI3K-AKT-mTOR signaling pathway. Among these, the ROS pathway regulates the proliferation and survival of tumor cells by modulating redox homeostasis, while excessive ROS accumulation can induce DNA damage and genetic instability, thereby facilitating tumor progression [46]. The PI3K-AKT-mTOR pathway, as a key regulator of cell growth, survival, and metabolism, is aberrantly activated in most OC and drives tumor cell proliferation and invasion [47]. Given their roles in cellular metabolism and survival, these pathways are likely pivotal in MARVELD1-mediated tumorigenesis. These pathways are likely pivotal in MARVELD1-mediated tumorigenesis. Additionally, cell function experiments reveal MARVELD1's capacity to enhance OC cell proliferation and migration.

This study provides new insights into MARVELD1's multifaceted role in promoting OC and highlights its potential as a therapeutic target. Future investigations will focus on the druggability of MARVELD1, exploring small molecule inhibitors, RNA interference (RNAi), and targeted delivery systems. Given that MARVELD1 affects the PI3K-AKT-mTOR pathway, indirect targeting via PI3K-AKT-mTOR inhibitors may offer a promising therapeutic strategy for patients with MARVELD1-high tumors. These approaches could open the door to novel therapies for OC.

The stability and clinical relevance of our four-gene prognostic model were confirmed through multidimensional validation. However, the lack of fully independent external validation may limit its generalizability. Future studies will incorporate additional public datasets and prospective clinical samples to enhance the external validation of the model.

Conclusion

In summary, the molecular mechanisms by which obesity-related genes contribute to the initiation and progression of OC were elucidated through integrative multi-omics analyses. The associations between obesity-related molecular subtypes and both immune and metabolic features were defined. A risk model centered on CXCL9, IGF2, FCGBP, and MARVELD1 was constructed, and the potential tumor-promoting pathways and clinical implications mediated by these genes were identified. The findings expanded the current understanding of

the impact of obesity on OC and suggested potential therapeutic targets and biomarkers for precision treatment in obese patients. Future studies should be undertaken to validate the clinical applicability of these findings and to explore targeted intervention strategies aimed at improving therapeutic outcomes and survival in obesity-associated OC.

Acknowledgements

This study was funded by Key Research and Development Program of Bozhou (BZZC2024013), Scientific Research Project of Gusu School of Nanjing Medical University (GSKY20210208 and GSKY20210203), Science Foundation of Jiangsu Province Grant (BK20240371), Cultivation Special Project of Gusu School of Nanjing Medical University (GSKY20220522), "Science and Education Revitalize Health" Youth Science and Technology Project of Suzhou (KJXW2020028), Special Project of Diagnosis and Treatment Technology for Key Clinical Diseases of Suzhou of Jiangsu Province (LCZX202013), and Science and Technology Project of Suzhou of Jiangsu Province (SYS2020175).

Disclosure of conflict of interest

None.

Address correspondence to: Dr. Yuting Liang, Center for Clinical Laboratory, The First Affiliated Hospital of Soochow University, No. 899, Pinghai Street, Suzhou 215002, Jiangsu, China; Molecular Oncology Laboratory, Department of Orthopedic Surgery and Rehabilitation Medicine, The University of Chicago Medical Center, Chicago, IL 60637, USA. E-mail: liangyuting666@126.com; Dr. Cong Shen, Center for Reproduction and Genetics, School of Gusu, The Affiliated Suzhou Hospital of Nanjing Medical University, Suzhou Municipal Hospital, Nanjing Medical University, Suzhou 215000, Jiangsu, China. E-mail: congshen@njmu.edu.cn; Dr. Shunyu Hou, Department of Obstetrics and Gynecology, The Affiliated Suzhou Hospital of Nanjing Medical University, Gusu School, Nanjing Medical University, Suzhou Municipal Hospital, Suzhou 215002, Jiangsu, China. E-mail: houshunyu@sina.com

References

[1] Kuroki L and Guntupalli SR. Treatment of epithelial ovarian cancer. BMJ 2020; 371: m3773.

[2] Guo H, Wei J, Zhang Y, Wang L, Wan J, Wang W, Gao L, Li J, Sun T and Ma L. Protein ubiquitination in ovarian cancer immunotherapy: the progress and therapeutic strategy. Genes Dis 2023; 11: 101158.

[3] Jiang C, Shen C, Ni M, Huang L, Hu H, Dai Q, Zhao H and Zhu Z. Molecular mechanisms of cisplatin resistance in ovarian cancer. Genes Dis 2023; 11: 101063.

[4] Grunewald T and Ledermann JA. Targeted therapies for ovarian cancer. Best Pract Res Clin Obstet Gynaecol 2017; 41: 139-152.

[5] Radu MR, Pradatu A, Duică F, Micu R, Cretoiu SM, Suciu N, Cretoiu D, Varlas VN and Radoi VE. Ovarian cancer: biomarkers and targeted therapy. Biomedicines 2021; 9: 693.

[6] Lee YT, Tan YJ and Oon CE. Molecular targeted therapy: treating cancer with specificity. Eur J Pharmacol 2018; 834: 188-196.

[7] Duan P, Fan L, Gao Q, Silwal BM, Ren M, Shen Y and Qu W. Targeted therapy of ovarian cancer with angiogenesis inhibitors. Curr Drug Targets 2017; 18: 1171-1178.

[8] Wang M, Chen L, Wang Y, Fan T, Zhu C, Li Z, Mou L, Yang H, Qian A and Li Y. CD147 facilitates cisplatin resistance in ovarian cancer through FOXM1 degradation inhibition. Genes Dis 2024; 11: 101277.

[9] Crudele L, Piccinin E and Moschetta A. Visceral adiposity and cancer: role in pathogenesis and prognosis. Nutrients 2021; 13: 2101.

[10] Kim B, Chung MJ, Park SW, Park JY, Bang S, Park SW, Song SY and Chung JB. Visceral obesity is associated with poor prognosis in pancreatic adenocarcinoma. Nutr Cancer 2016; 68: 201-207.

[11] Nitsche L, Vedire Y, Kannisto E, Wang X, Seager RJ, Pabla S, Patnaik SK and Yendamuri S. Visceral obesity in non-small cell lung cancer. Cancers (Basel) 2022; 14: 3450.

[12] Xiao J, Mazurak VC, Olobatuyi TA, Caan BJ and Prado CM. Visceral adiposity and cancer survival: a review of imaging studies. Eur J Cancer Care (Engl) 2018; 27: e12611.

[13] Zhang Y, Nowicka A, Solley TN, Wei C, Parikh A, Court L, Burks JK, Andreeff M, Woodward WA, Dadbin A, Kolonin MG, Lu KH and Klopp AH. Stromal cells derived from visceral and obese adipose tissue promote growth of ovarian cancers. PLoS One 2015; 10: e0136361.

[14] Heus C, Smorenburg A, Stoker J, Rutten MJ, Amant FCH and van Lonkhuijzen LRCW. Visceral obesity and muscle mass determined by CT scan and surgical outcome in patients with advanced ovarian cancer. A retrospective cohort study. Gynecol Oncol 2021; 160: 187-192.

[15] Wilkerson MD and Hayes DN. ConsensusClusterPlus: a class discovery tool with confidence

assessments and item tracking. Bioinformatics 2010; 26: 1572-1573.
[16] Yoshihara K, Shahmoradgoli M, Martínez E, Vegesna R, Kim H, Torres-Garcia W, Treviño V, Shen H, Laird PW, Levine DA, Carter SL, Getz G, Stemke-Hale K, Mills GB and Verhaak RG. Inferring tumour purity and stromal and immune cell admixture from expression data. Nat Commun 2013; 4: 2612.
[17] Song B, Chi H, Peng G, Song Y, Cui Z, Zhu Y, Chen G, Wu J, Liu W, Dong C, Wang Y, Xu K, Yu Z and Song B. Characterization of coagulation-related gene signature to predict prognosis and tumor immune microenvironment in skin cutaneous melanoma. Front Oncol 2022; 12: 975255.
[18] Jiang P, Gu S, Pan D, Fu J, Sahu A, Hu X, Li Z, Traugh N, Bu X, Li B, Liu J, Freeman GJ, Brown MA, Wucherpfennig KW and Liu XS. Signatures of T cell dysfunction and exclusion predict cancer immunotherapy response. Nat Med 2018; 24: 1550-1558.
[19] Li XY, Zhao ZJ, Wang JB, Shao YH, Hui-Liu, You JX and Yang XT. m7G Methylation-related genes as biomarkers for predicting overall survival outcomes for hepatocellular carcinoma. Front Bioeng Biotechnol 2022; 10: 849756.
[20] Yu G, Wang LG, Han Y and He QY. clusterProfiler: an R package for comparing biological themes among gene clusters. OMICS 2012; 16: 284-287.
[21] Geeleher P, Cox N and Huang RS. pRRophetic: an R Package for prediction of clinical chemotherapeutic response from tumor gene expression levels. PLoS One 2014; 9: e107468.
[22] Song B, Wu P, Liang Z, Wang J, Zheng Y, Wang Y, Chi H, Li Z, Song Y, Yin X, Yu Z and Song B. A novel necroptosis-related gene signature in skin cutaneous melanoma prognosis and tumor microenvironment. Front Genet 2022; 13: 9171007.
[23] Wu Z, Hou Q, Chi H, Liu J, Mei Y, Chen T, Yang K, Zheng J, Xu J, Wei F and Wang L. Single-cell RNA sequencing reveals a distinct profile of bone immune microenvironment and decreased osteoclast differentiation in type 2 diabetic mice. Genes Dis 2024; 11: 101145.
[24] Ren R, Chen Y, Zhou Y, Shen L, Chen Y, Lei J, Wang J, Liu X, Zhang N, Zhou D, Zhao H and Li Y. STIM1 promotes acquired resistance to sorafenib by attenuating ferroptosis in hepatocellular carcinoma. Genes Dis 2024; 11: 101281.
[25] Rowan CR, McManus J, Boland K and O'Toole A. Visceral adiposity and inflammatory bowel disease. Int J Colorectal Dis 2021; 36: 2305-2319.
[26] Iacobellis G, Penaherrera CA, Bermudez LE and Bernal Mizrachi E. Admission hyperglycemia and radiological findings of SARS-CoV2 in patients with and without diabetes. Diabetes Res Clin Pract 2020; 164: 108185.
[27] Cariello M, Piccinin E, Pasculli E, Arconzo M, Zerlotin R, D'Amore S, Mastropasqua F, Peres C, Graziano G, Villani G, Pesole G and Moschetta A. Platelets from patients with visceral obesity promote colon cancer growth. Commun Biol 2022; 5: 553.
[28] Freuer D, Linseisen J, O'Mara TA, Leitzmann M, Baurecht H, Baumeister SE and Meisinger C. Body fat distribution and risk of breast, endometrial, and ovarian cancer: a two-sample mendelian randomization study. Cancers (Basel) 2021; 13: 5053.
[29] Prat J. New insights into ovarian cancer pathology. Ann Oncol 2012; 23 Suppl 10: x111-x117.
[30] Tossetta G and Inversetti A. Ovarian cancer: advances in pathophysiology and therapies. Int J Mol Sci 2023; 24: 8930.
[31] Zhao FY, Zhang Q, Wang JM, Jiang JY, Huyan LY, Liu BQ, Yan J, Li C and Wang HQ. BAG3 epigenetically regulates GALNT10 expression via WDR5 and facilitates the stem cell-like properties of platin-resistant ovarian cancer cells. Biochim Biophys Acta Mol Cell Res 2021; 1868: 119077.
[32] Liu Y, Cao H, Zhao Y, Shan L and Lan S. Fisetin-induced cell death in human ovarian cancer cell lines via zbp1-mediated necroptosis. J Ovarian Res 2022; 15: 57.
[33] Razis E, Kalogeras KT, Kotsantis I, Koliou GA, Manousou K, Wirtz R, Veltrup E, Patsea H, Poulakaki N, Dionysopoulos D, Pervana S, Gogas H, Koutras A, Pentheroudakis G, Christodoulou C, Linardou H, Pavlakis K, Koletsa T, Pectasides D, Zagouri F and Fountzilas G. The role of CXCL13 and CXCL9 in early breast cancer. Clin Breast Cancer 2020; 20: e36-e53.
[34] Livingstone C. IGF2 and cancer. Endocr Relat Cancer 2013; 20: R321-339.
[35] Wang K, Guan C, Shang X, Ying X, Mei S, Zhu H, Xia L and Chai Z. A bioinformatic analysis: the overexpression and clinical significance of FCGBP in ovarian cancer. Aging (Albany NY) 2021; 13: 7416-7429.
[36] Wang S, Li Y, Han F, Hu J, Yue L, Yu Y, Zhang Y, He J, Zheng H, Shi S, Fu X and Wu H. Identification and characterization of MARVELD1, a novel nuclear protein that is down-regulated in multiple cancers and silenced by DNA methylation. Cancer Lett 2009; 282: 77-86.
[37] Wu Y, Biswas D and Swanton C. Impact of cancer evolution on immune surveillance and checkpoint inhibitor response. Semin Cancer Biol 2022; 84: 89-102.
[38] Coukos G, Tanyi J and Kandalaft LE. Opportunities in immunotherapy of ovarian cancer. Ann Oncol 2016; 27 Suppl 1: i11-i15.

[39] Hatta M, Nagai H, Okino K, Onda M, Yoneyama K, Ohta Y, Nakayama H, Araki T and Emi M. Down-regulation of members of glycolipid-enriched membrane raft gene family, MAL and BENE, in cervical squamous cell cancers. J Obstet Gynaecol Res 2004; 30: 53-58.

[40] Shao L, Cui Y, Li H, Liu Y, Zhao H, Wang Y, Zhang Y, Ng KM, Han W, Ma D and Tao Q. CMTM5 exhibits tumor suppressor activities and is frequently silenced by methylation in carcinoma cell lines. Clin Cancer Res 2007; 13: 5756-5762.

[41] Mimori K, Shiraishi T, Mashino K, Sonoda H, Yamashita K, Yoshinaga K, Masuda T, Utsunomiya T, Alonso MA, Inoue H and Mori M. MAL gene expression in esophageal cancer suppresses motility, invasion and tumorigenicity and enhances apoptosis through the Fas pathway. Oncogene 2003; 22: 3463-3471.

[42] Liu W, Dong Y, Guo R, Zhou D, Qin Y, Ma Y, Zhang J and Li A. MARVELD1 inhibits Neuro2a cell migration and tumorigenesis via regulating the transcriptional coactivators and protein methylation. Bull Cancer 2025; 112: 458-468.

[43] Luo X and Gao Z. MARVELD1 promotes the invasiveness in pancreatic adenocarcinoma through the activation of epithelial-to-mesenchymal transition. Protein Pept Lett 2025; 32: 224-233.

[44] Xia L, Jin P, Tian W, Liang S, Tan L and Li B. Up-regulation of MARVEL domain-containing protein 1 (MARVELD1) accelerated the malignant phenotype of glioma cancer cells via mediating JAK/STAT signaling pathway. Braz J Med Biol Res 2021; 54: e10236.

[45] Li L, Zhang W, Sun Y, Zhang W, Lu M, Wang J, Jin Y and Xi Q. A clinical prognostic model of oxidative stress-related genes linked to tumor immune cell infiltration and the prognosis of ovarian cancer patients. Heliyon 2024; 10: e28442.

[46] Son Y, Han M, Wu X and Roh YS. SIRT1-mediated redox and senescence regulation in cancer: mechanisms and therapeutic implications. Antioxidants (Basel) 2025; 14: 1076.

[47] Pourbarkhordar V, Rahmani S, Roohbakhsh A, Hayes AW and Karimi G. Melatonin effect on breast and ovarian cancers by targeting the PI3K/Akt/mTOR pathway. IUBMB Life 2024; 76: 1035-1049.

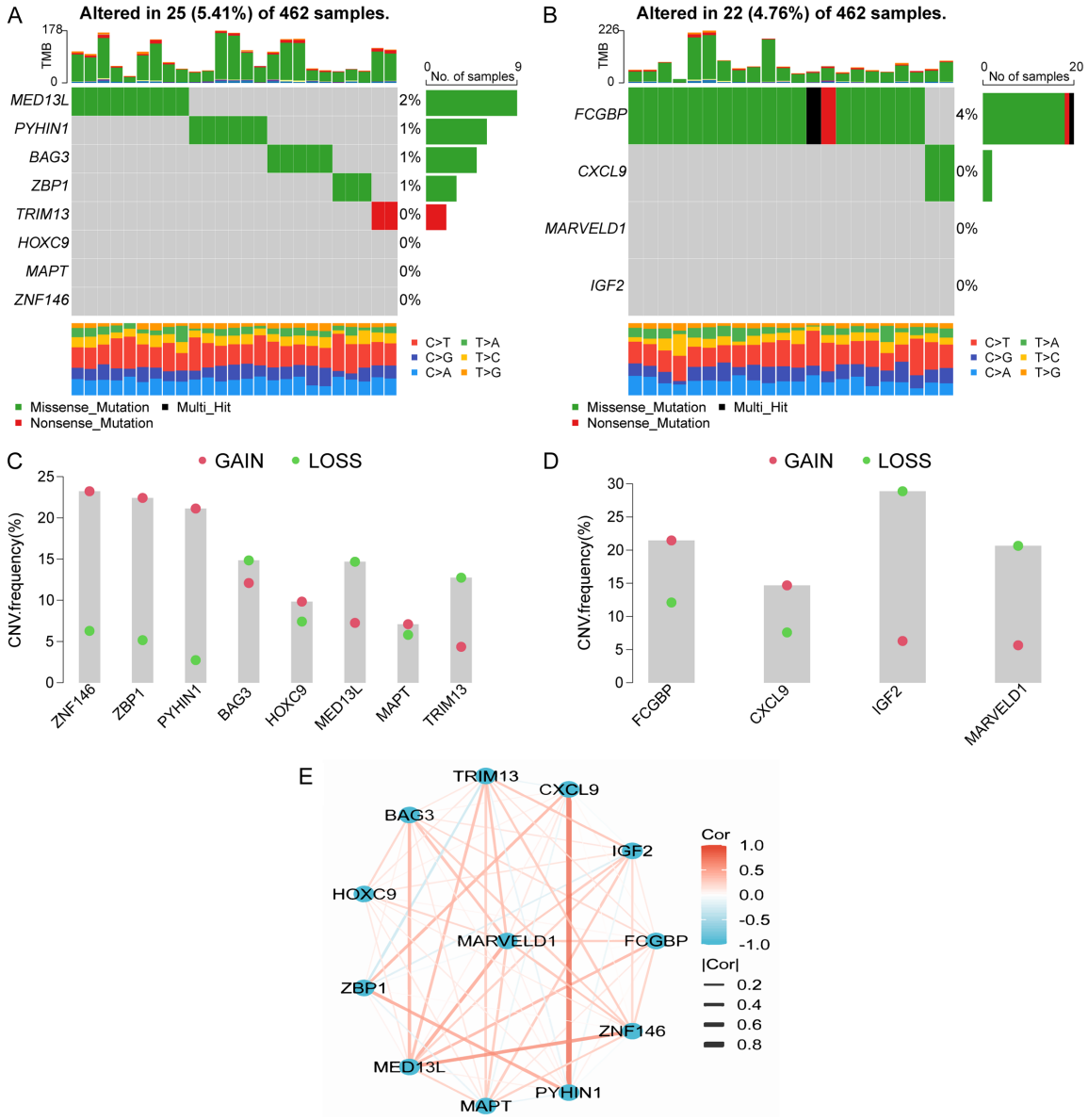

Figure S1. Genetic and transcriptional variations of VORGs and OC core prognostic genes. A. Genetic variation landscape of eight VORGs in 462 OC patients from the The Cancer Genome Atlas (TCGA) cohort. B. Genetic variation landscape of four core prognostic genes in 462 OC patients from the TCGA cohort. C. Copy number variation (CNV) analysis of the eight VORGs, with ZNF146 displaying the most frequent amplifications, while BAG3 and MED13L showed the highest deletion rates. D. CNV analysis of the four core prognostic genes, with FCGBP displaying the most frequent amplifications, while IGF2 showed the highest deletion rates. E. The network reflected the relationship between VORGs and OC core prognostic genes, with MARVELD1 occupying a central position in the network.

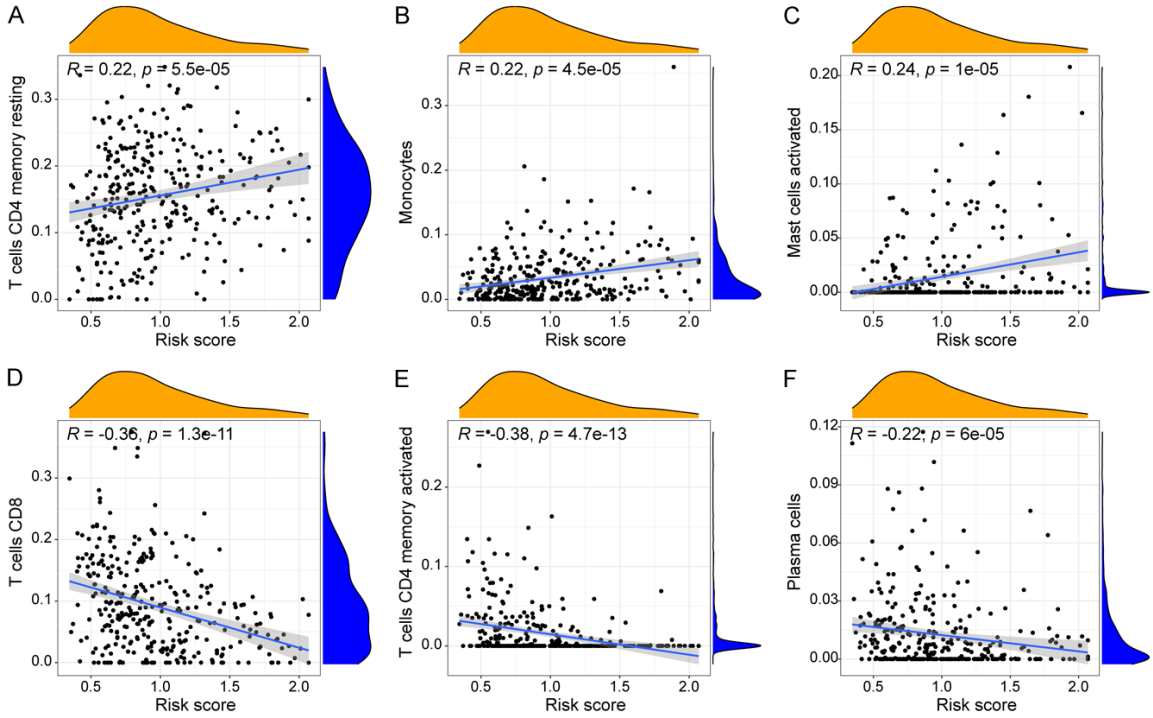

Figure S2. Correlation between risk score and immune cell infiltration. A-C. Risk score was positively correlated with resting CD4 memory T cells, monocytes, and activated mast cells infiltration. D-F. Risk score was negatively correlated with CD8 T cells, activated CD4 memory T cells, and plasma cells infiltration.